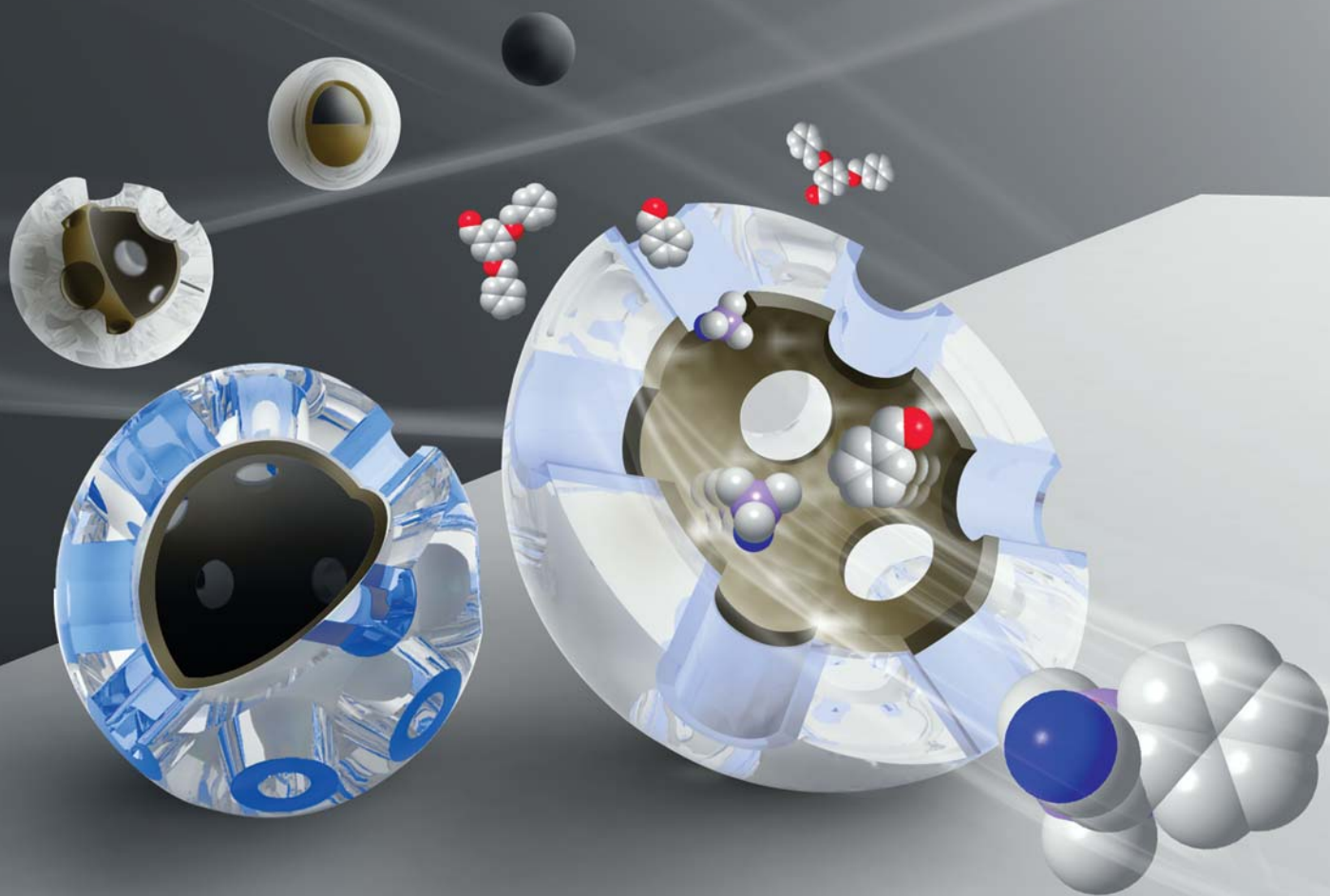


# Journal of Materials Chemistry

www.rsc.org/materials

Volume 20 | Number 47 | 21 December 2010 | Pages 10555–10766



ISSN 0959-9428

RSC Publishing

**PAPER**

R. M. Anisur *et al.*

Hollow silica nanosphere having functionalized interior surface with thin manganese oxide layer: nanoreactor framework for size-selective Lewis acid catalysis



0959-9428 (2010) 20:47;1-E

# Hollow silica nanosphere having functionalized interior surface with thin manganese oxide layer: nanoreactor framework for size-selective Lewis acid catalysis†

Rahman Md Anisur, Jongmin Shin, Hyung Ho Choi, Kyung Min Yeo, Eun Joo Kang\* and In Su Lee\*

Received 12th August 2010, Accepted 22nd September 2010

DOI: 10.1039/c0jm02647f

A novel selective nanoscale etching process that generated a well defined hollow nanostructure was developed by treating manganese oxide nanoparticles with a hydroxylamine solution. This selective etching process was used for exploiting a novel method of differentially functionalizing the internal surface of a hollow silica shell with a catalytically active  $\text{Mn}_3\text{O}_4$  layer and creating a novel nanoreactor framework. The nanoreactor fabricated by the newly developed method catalyzed the cyanosilylation reactions of various aromatic aldehydes with size and shape selectivity. Moreover, the substrate selectivity in the cyanosilylation reactions was efficiently tuned by modifying the outer silica shell with silane coupling reagents.

## 1 Introduction

Hollow inorganic nanoparticles are attractive candidates for emergent applications, including catalysis, drug delivery vehicles, contrast agents for molecular imaging, and energy and gas storage materials owing to their superior properties, such as large surface area and ability to provide a colloid with a protected interior cavity suitable for selectively encapsulating molecules.<sup>1,2</sup> In this context, we previously developed hollow manganese oxide nanoparticles with multi-functionality for simultaneous MR imaging and drug delivery.<sup>2a</sup> Considerable effort has been devoted to improve the quality and uniformity of their hollow interior structure. While recent developments of several synthetic methods allow the production of various hollow inorganic nanoparticles, precise control of their phase, structure, surface and consequent properties is a significant challenge.<sup>3,4</sup> In particular, for further development of nanoreactors with enhanced selectivity, it is important to devise a new method for functionalizing the interior surface, which will allow molecular recognition and chemical reactions to occur only inside the hollow shell.<sup>2c,e,4e,5</sup>

This paper reports our recent findings on the generation of well defined hollow nanostructures of manganese oxide nanoparticles through a selective nanoscale etching process in a hydroxylamine dispersion and the use of this process for exploiting a novel method of differentially functionalizing the internal surface of a hollow silica shell with a catalytically active  $\text{Mn}_3\text{O}_4$  layer. Several significant attempts were recently made to functionalize the hollow interior space using a template etching process or nanoscale Kirkendall effect.<sup>6</sup> In most cases, these processes lead to the incorporation of single or multiple numbers of catalytic nanoparticles inside the cavity of the hollow sphere. However, little attention has been directed towards a method for coating

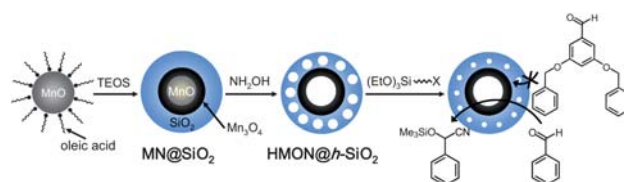
the entire cavity surface with a thin catalytic layer, which might be more desirable for providing a large catalytic surface area and producing a different interior environment of hollow sphere distinct to that of the exterior surface.<sup>7</sup>

In this study, hollow nanospheres fabricated using the newly developed method were used successfully as a nanoreactor that could selectively catalyze cyanosilylation reactions of aromatic aldehydes. A substantial improvement in their size-selectivity was demonstrated, which was achieved by controlling the porosity of the silica shell using an appropriate silane modification. Scheme 1 shows the approach to fabricating a nanoreactor composed of a hollow and porous silica shell and a functionalized interior surface with a thin  $\text{Mn}_3\text{O}_4$  layer and optimizing its catalytic performance.

## 2 Results and discussion

### 2.1 Generation of hollow manganese oxide nanoparticle via nanoscale etching process

The  $\text{MnO}$ – $\text{Mn}_3\text{O}_4$  core–shell nanoparticles (CSNPs), which were used as a sacrificial template, were prepared by coating oleic acid-stabilized  $\text{MnO}$  nanoparticles with a Pluronic copolymer (F127,  $\text{PEO}_{19}$ – $\text{PPO}_{69}$ – $\text{PEO}_{19}$ ) and inducing surface oxidation in the aqueous dispersion by air (Fig. 1).<sup>2a,8</sup> To remove the core part from the CSNP, a hydroxylamine ( $\text{NH}_2\text{OH}$ ) solution with metal ion complexing ability was tested for use as an etchant. The  $\text{NH}_2\text{OH}$ -based solutions are used frequently for the selective extraction of manganese ions from oxide minerals.<sup>9</sup> When a  $\text{NH}_2\text{OH}$  solution (2.5 M) was added to a 1.0 mL aqueous



Scheme 1 Fabrication and modification of  $\text{HMON}@h\text{-SiO}_2$ .

Department of Applied Chemistry, College of Applied Science, Kyung Hee University, Gyeonggi-do, 449-701, Korea. E-mail: ejkang24@khu.ac.kr; insulee97@khu.ac.kr; Fax: +82-31-202-7337; Tel: +82-31-201-3823

† Electronic supplementary information (ESI) available: Additional TEM images and NMR data. See DOI: 10.1039/c0jm02647f

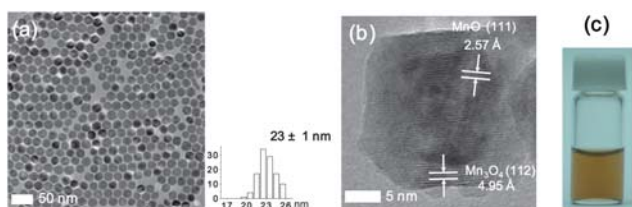


**Fig. 1** (a) TEM and (b) HRTEM images of CSNPs. A histogram shows the size distribution. (c) A picture showing the dispersion containing CSNPs.

dispersion of the CSNPs ( $0.5 \text{ mg mL}^{-1}$ ) and stirred at room temperature and pH 9, the dark brown color of the initial dispersion faded gradually over a few days to generate a light brown dispersion. Transmission electron microscopy (TEM), high resolution TEM (HRTEM), and scanning electron microscopy (SEM) of the nanoparticles isolated from the dispersion after a 24 h reaction showed that the core part of the MnO phase was carved selectively away from most of the CSNPs, and a spherical void was left inside the thin and uniform  $\text{Mn}_3\text{O}_4$  shell with a  $2.5(\pm 0.4) \text{ nm}$  thickness (Fig. 2). It was observed that 79% CSNPs had transformed into hollow manganese oxide nanoparticles (HMONS) with inner and outer diameters of  $21(\pm 2) \text{ nm}$  and  $16(\pm 2) \text{ nm}$ , respectively. The generation of a hollow structure composed mainly of  $\text{Mn}_3\text{O}_4$  is also supported by the nitrogen adsorption/desorption isotherm exhibiting a narrow pore size distribution centered at 15 nm and a magnetic hysteresis loop with much higher saturation magnetization at 5 K (Fig. 3). HMION formation can be explained by the higher MnO dissolution rate than  $\text{Mn}_3\text{O}_4$  in complex formation between manganese ions and  $\text{NH}_2\text{OH}$ . The control experiment carried out with  $\text{Mn}_3\text{O}_4$  nanoparticles in a  $\text{NH}_2\text{OH}$  solution did not allow significant changes in the nanoparticles

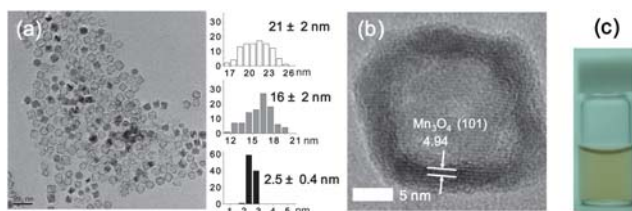


**Fig. 2** (a) TEM image of the sample obtained from the reaction of CSNP and  $\text{NH}_2\text{OH}$  for 24 h. A histogram showing the size distribution of the outer (white) and inner (grey) diameters and shell thickness (black) of HMONS. (b) HRTEM image of HMION. (c) A picture showing the dispersion containing 79% HMION and 21% CSNP.

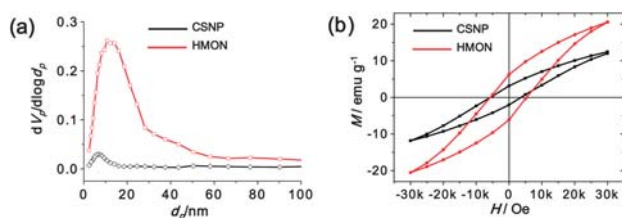


**Fig. 3** (a) Pore size distribution of CSNP and HMION derived by using BJH model based on their  $\text{N}_2$  sorption isotherms. (b) Field dependent magnetization of CSNP and HMION at 5 K.

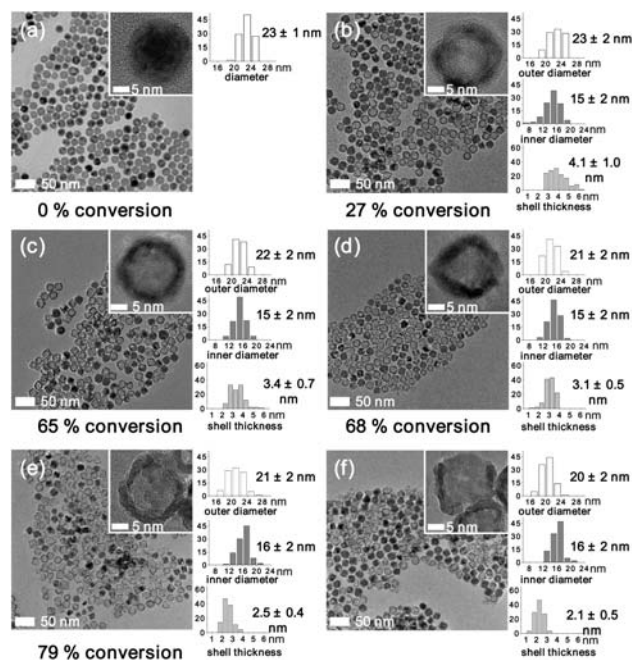


**Fig. 4** TEM and HRTEM (insets) images of the samples obtained from the dispersion of CSNP and  $\text{NH}_2\text{OH}$  after reaction for (a) 10 min, (b) 1 h, (c) 6 h, (d) 12 h, (e) 24 h, and (f) 5 days. Histograms show the size distribution of outer (white) and inner (grey) diameters and shell thickness (black).

(ESI $^\dagger$ ). The solubilities of bulk MnO (Aldrich,  $\sim 60$  mesh, 99%) and  $\text{Mn}_3\text{O}_4$  (Aldrich,  $\sim 325$  mesh, 99%) powders in 2.5 M  $\text{NH}_2\text{OH}$  ( $\text{p}K_b = 8.04$ ) solution were determined to be  $8.3 \text{ mg mL}^{-1}$  and  $3 \times 10^{-3} \text{ mg mL}^{-1}$ , respectively, which suggest much easier dissolution of MnO than  $\text{Mn}_3\text{O}_4$ . The TEM images of the samples obtained from the reaction dispersion of CSNP and  $\text{NH}_2\text{OH}$  at different times showed that a hollow interior had developed in 27% of nanoparticles at 1 h. As the reaction proceeded, the number of CSNPs transforming into the hollow structure increased, reaching a 79% conversion yield at 24 h (Fig. 4). Whilst the hollow interior structure had not changed significantly up to 24 h, the shell thickness of the as-formed HMONS decreased gradually with increasing reaction time from  $4(\pm 1) \text{ nm}$  at 1 h to  $2.5(\pm 0.4) \text{ nm}$  at 24 h. Treatment for a longer period of time resulted in a thinner HMION with broken shell, whereas some CSNPs with solid interior remained, which is consistent with the decrease but still presence of the MnO peaks in the XRD pattern, even after a 5 day reaction (Fig. 5). The above observations can be explained by the slow diffusion of the  $\text{NH}_2\text{OH}$  solution along the crystalline grain boundaries of the  $\text{Mn}_3\text{O}_4$  shell followed by rapid and complete etching of the MnO core immediately upon entering the core part. This suggests that the time required for HMION conversion might be dependent on the grain boundary structure in the shell of each CSNPs.

## 2.2 Synthesis of hollow silica nanosphere with $\text{Mn}_3\text{O}_4$ functionalized interior surface

The current synthetic method of the hollow structure was used to functionalize the internal surface of a hollow silica sphere. The selective removal of the MnO core inside the silica sphere would

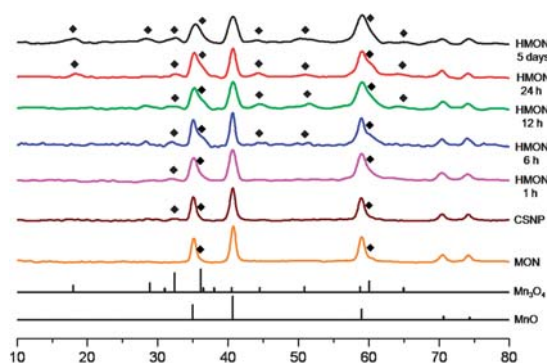


**Fig. 5** XRD patterns of the samples obtained over time from the reaction dispersion of CSNP and  $\text{NH}_2\text{OH}$ . The diffraction peaks from  $\text{Mn}_3\text{O}_4$  phase were marked with black diamonds. The lines below show the position of the reflections corresponding to cubic MnO phase (JCPDS Card No. 07-0230) and the tetragonal  $\text{Mn}_3\text{O}_4$  phase (JCPDS Card No. 24-0734).

provide a silica sphere with a void space and an interior surface coated with a  $\text{Mn}_3\text{O}_4$  layer. For this purpose,  $38(\pm 4)$  nm sized silica spheres encapsulating  $20(\pm 3)$  nm sized manganese oxide nanoparticles stabilized by oleic acid ( $\text{Mn@SiO}_2$ ) were prepared using a modified reverse microemulsion technique followed by a treatment with a 0.5 M  $\text{NH}_2\text{OH}$  solution using a similar procedure to that applied for HMION synthesis (Fig. 6). The analyses of the spheres isolated after 24 h reaction by TEM, HRTEM, and SEM showed that the MnO core had been removed completely from the  $\text{Mn@SiO}_2$  and a thin  $\text{Mn}_3\text{O}_4$  layer was left covering the newly created surface of the hollow interior (Fig. 7 and 8). Unlike the CSNPs, dissolution of the MnO core and interior void formation occurred for all  $\text{Mn@SiO}_2$ s in the reaction dispersion, resulting in the synthesis of homogeneous products with a hollow structure. The complete dissolution of the MnO phase is also supported by the absence of any MnO peaks in the XRD pattern (Fig. 9b). Dissolution of the MnO core was accompanied by partial etching of the silica shell, leading to the formation of  $\text{HMION@h-SiO}_2$  composed of a hollow and porous silica shell with inner and outer diameters of  $19(\pm 3)$  nm and  $38(\pm 4)$  nm, respectively, and an interior surface coated with a  $3.6(\pm 0.8)$  nm  $\text{Mn}_3\text{O}_4$  layer. The generation of porous silica under basic conditions has been reported.<sup>10</sup> The pore size distribution centered at 1 nm, which was derived by using HK model based on the nitrogen adsorption/desorption isotherm of  $\text{HMION@h-SiO}_2$ , also supports the formation of nanopores at the silica shell during the treatment in the  $\text{NH}_2\text{OH}$  dispersion

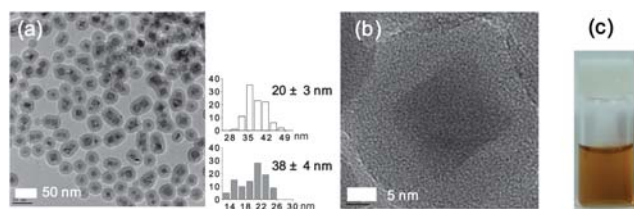


**Fig. 6** (a) TEM and (b) HRTEM images of  $\text{Mn@SiO}_2$ . Histograms show the size distribution of outer (white) and inner (grey) diameters. (c) A picture showing the dispersion containing  $\text{Mn@SiO}_2$ .

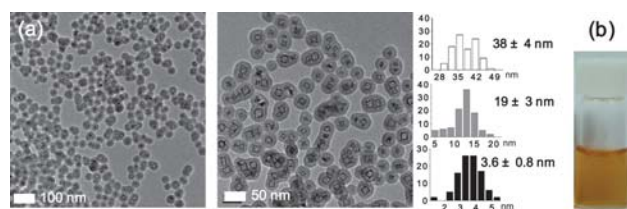


**Fig. 7** (a) TEM images of  $\text{HMION@h-SiO}_2$ . Histograms show the size distribution of outer (white) and inner (grey) diameters and shell thickness (black). (b) A picture showing the dispersion containing  $\text{HMION@h-SiO}_2$ .

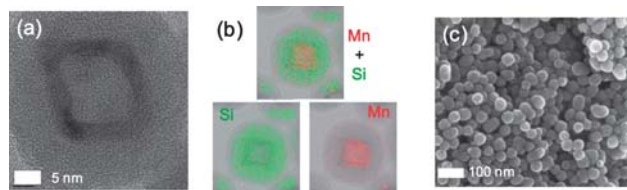


**Fig. 8** (a) A HRTEM image, (b) EDX elementary maps, and (c) a SEM image of  $\text{HMION@h-SiO}_2$ .

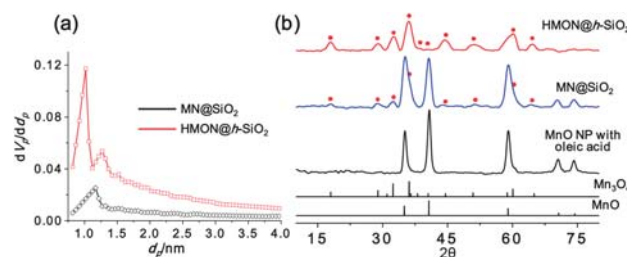


**Fig. 9** (a) Pore size distribution of  $\text{Mn@SiO}_2$  and  $\text{HMION@h-SiO}_2$  derived by using HK model based on their  $\text{N}_2$  sorption isotherms. (b) XRD patterns of MnO NP stabilized by oleic acid,  $\text{Mn@SiO}_2$ , and  $\text{HMION@h-SiO}_2$ . The lines below show the position of the reflections corresponding to cubic MnO phase (JCPDS Card No. 07-0230) and the tetragonal  $\text{Mn}_3\text{O}_4$  phase (JCPDS Card No. 24-0734).

(Fig. 9a). Based on the resulting hollow structure of the  $\text{HMION@h-SiO}_2$ , it was envisioned that a reaction catalyzed by a Lewis acid could be allowed only for molecules that diffuse into the cavity surface rapidly through the porous silica shell. Therefore, the hollow nanoparticle could act as a nanoreactor with enhanced size and shape selectivity. In addition, the selectivity and reactivity of the nanoreactor can be controlled by selectively modifying either the interior surface or outer silica shell due to the distinct difference in their chemical characteristics.

### 2.3 Evaluation of catalytic activity of the $\text{HMION@h-SiO}_2$ s in cyanosilylation reactions

In order to evaluate the effectiveness of the  $\text{HMION@h-SiO}_2$ s as a nanoreactor for selective catalytic reactions, this study examined the first hollow nanoparticle catalyzed cyanosilylation of carbonyl substrates.<sup>11</sup> In the experimental setup, a solution of benzaldehyde (**3a**) and cyanotrimethylsilane (2.0 equiv.) in  $\text{CH}_2\text{Cl}_2$  was treated with 5 mol% of  $\text{HMION@h-SiO}_2$  (**1**) at

ambient temperature. This trial run afforded the cyanohydrin trimethylsilyl ether in 99% yield after stirring for 12 h. In the  $^1\text{H}$  NMR spectrum to check the conversion yield, the peak at 10.02 ppm ( $\text{PhCHO}$ ) disappeared completely and a new peak at 5.50 ppm ( $\text{PhCHCN}(\text{OTMS})$ ) was observed ( $\text{ESI}^\dagger$ ). The control experiment with the  $\text{Mn@SiO}_2$  catalyst, having a non-porous silica shell, showed no conversion at all, confirming the importance of the pores in the silica shell of  $\text{HMON@h-SiO}_2$  as a path for the reactant molecules to access the catalytically active manganese oxide core. More importantly, the comparison results of the reactions with 1 mol% of  $\text{HMON@h-SiO}_2$  and  $\text{Mn}_3\text{O}_4@\text{-p-SiO}_2$  having a non-hollow  $\text{Mn}_3\text{O}_4$  core surrounded by a porous silica shell, showing 76% (31%) and 9% (1%) conversion yields after 12 h (3 h), strongly implying that the cyanosilylation reactions efficiently occurred in the hollow interior surface of manganese oxide nanostructure. Catalytic recyclability was checked for three times with the same batch of catalyst, and the observed yields in three consecutive runs were 99%, 99%, and 88%, respectively. The TEM analyses of the recovered catalysts from the third run showed the preservation of the size and shape of the initial  $\text{HMON@h-SiO}_2$  ( $\text{ESI}^\dagger$ ). In addition, any leaching of Mn ions was not detected in the ICP analyses of the supernatant solutions collected after each run.

The same reaction performed with biphenyl-4-carboxaldehyde (**3b**) and 3,5-bis(benzyloxy)benzaldehyde (**3f**) afforded the corresponding cyanohydrins in 99% and 97% yields, respectively. However, the conversion yields for 1-naphthaldehyde (**3c**) and 1-pyrenecarboxaldehyde (**3d**) were slightly lower (<90%), and the reaction of 9-anthraldehyde (**3e**) reached only 43% yield. In the case of the reaction of 9-anthraldehyde, 9,10-endoperoxy anthraldehyde and the corresponding cyanohydrin trimethylsilyl ether were produced as byproducts. This result led us to theorize that size of the substrates acts as a crucial variable for determining the progress of  $\text{HMON@h-SiO}_2$ -catalyzed cyanosilylation reactions by influencing the diffusion rate through the pores of the silica shell.<sup>12</sup> In addition, its catalytic propensity is dependent on the presence of  $\alpha$ -substituents in the aromatic substrate, rather than their entire molecular dimensions.

#### 2.4 Improvement of catalytic selectivity by the surface modification of silica shell

Encouraged by the size-selectivity observed for the cyanosilylation reactions, it was assumed that the substrate selectivity could be tuned efficiently by modifying either the interior surface or outer silica shell. For this purpose,  $\text{HMON@h-SiO}_2$  was treated with various silane reagents, including (3-aminopropyl)trimethoxysilane, *n*-propyltrimethoxysilane, (2-phenylethyl)trimethoxysilane and *n*-octadecyltrimethoxysilane, which

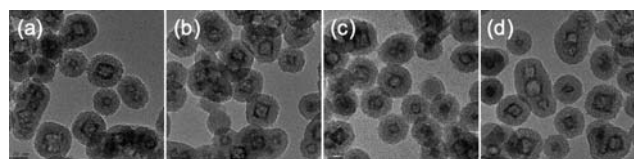


**Fig. 10** TEM images of the modified  $\text{HMON@h-SiO}_2$  catalysts with (a) 3-aminopropyl (**2a**), (b) *n*-propyl (**2b**), (c) 2-phenylethyl (**2c**), and (d) octadecyl (**2d**) groups.

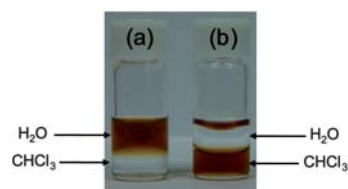


**Fig. 11** Pictures showing the dispersity of (a)  $\text{HMON@h-SiO}_2$  (**1**) and (b) octadecyl-modified  $\text{HMON@h-SiO}_2$  (**2d**) between two immiscible phases of water (upper layer) and chloroform (lower layer).

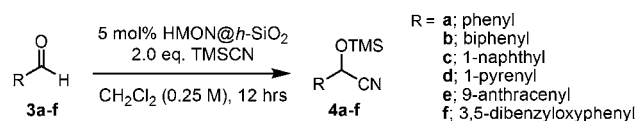
reacted with the surface silanol group to produce modified  $\text{HMON@h-SiO}_2$  catalysts with 3-aminopropyl (**2a**), *n*-propyl (**2b**), 2-phenylethyl (**2c**), and *n*-octadecyl (**2d**) groups, respectively. TEM analyses did not show any significant change in the size and shape of the initial  $\text{HMON@h-SiO}_2$  after the silane modification (Fig. 10). While the 3-aminopropyl-, *n*-propyl-, and 2-phenylethyl-modified particles are well dispersible in ethanol or ethanol/water mixture solvent, *n*-octadecyl-modified particles show much better dispersibility in chloroform compared with ethanol or ethanol/water mixture (Fig. 11).

The catalytic reactivity of the modified  $\text{HMON@h-SiO}_2$  catalysts towards sterically differentiated aromatic substrates was examined. As summarized in Table 1, all substrates treated with the modified  $\text{HMON@h-SiO}_2$  catalysts, **2a-d**, had lower yields than those with **1**, presumably the result of the reduced nanopore size in the interior silica shell. However, the rate of decrease in yield was affected by both the molecular shape and dimensions. For example, the 3-aminopropyl and *n*-propyl-modified catalysts (**2a,b**) showed slightly lower catalytic activity, and the rate of decrease in yield was enhanced in the reactions of large-dimension substrates, such as **3d** and **3e**, with 53% and 60%, respectively. When the *n*-octadecyl-modified  $\text{HMON@h-SiO}_2$  catalyst **2d** was used in the cyanosilylation reaction, the catalytic activity towards aromatic aldehydes except benzaldehyde was decreased dramatically (more than 70%) compared with that of **2b**. In particular, reactions with **3f** resulted in only 7% yield, representing a significant size-selective reaction in a porous nanoreactor. To demonstrate the competition between

**Table 1** Cyanosilylation of aromatic aldehydes over various  $\text{HMON@h-SiO}_2$  catalysts<sup>a</sup>

Catalyst	Yield <sup>b</sup> (%)					
	<b>4a</b>	<b>4b</b>	<b>4c</b>	<b>4d</b>	<b>4e</b>	<b>4f</b>
<b>1</b>	99	99	83	90	43	97
<b>2a</b>	93	81	77	42	17	75
<b>2b</b>	92	86	70	38	10	81
<b>2c</b>	61	58	57	29	14	54
<b>2d</b>	46	20	35	11	4	7

<sup>a</sup> Conditions: aldehyde (0.5 mmol), TMSCN (1.0 mmol),  $\text{CH}_2\text{Cl}_2$  (0.25 M), catalyst (0.025 mmol, based on Mn contents), room temperature, under  $\text{N}_2$ .  
<sup>b</sup> Determined by  $^1\text{H}$  NMR based on the carbonyl substrate.



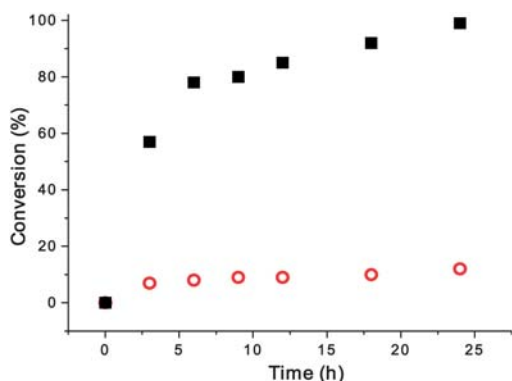


**Fig. 12** Conversion of benzaldehyde (solid square) and 3,5-bis(benzyloxy)benzaldehyde (open circle) in cyanosilylation reaction with octadecyl-modified **HMON@*h*-SiO<sub>2</sub>** catalyst (**2d**) groups.

a small and a large substrate molecule for access to the catalytically active Mn cores of catalyst, two differently sized aldehydes, both benzaldehyde (**3a**) and 3,5-bis(benzyloxy)benzaldehyde (**3f**), were added to the reaction mixture, and the conversion of aldehydes was monitored by the <sup>1</sup>H NMR spectra (Fig. 12). The treatment of the two aldehydes with the *n*-octadecyl-modified catalyst, **2d**, showed great substrate discrimination by increasing the relative reaction rate in favor of the smaller benzaldehyde, resulting in the quantitative transformation of **3a** but only 12% conversion of **3f**.

### 3 Experimental

#### 3.1 Preparation and modification of **HMON@*h*-SiO<sub>2</sub>**

**General consideration.** All reagents including MnCl<sub>2</sub>·4H<sub>2</sub>O (Aldrich), sodium oleate (TCI), oleic acid (Aldrich), pluronic F127 (BASF), 1-octadecene (Aldrich), hydroxylamine (Aldrich), cyclohexane, NH<sub>4</sub>OH (Samchun chem.), tetraethyl orthosilicate (Acros), Igepal CO-520 (Acros), oleylamine (Acros), manganese acetylacetonate (STREM), *n*-propyltrimethoxysilane, *n*-octadecyltrimethoxysilane, (2-phenylethyl)trimethoxysilane, 3-aminopropyltrimethoxysilane (Gelest), MnO (Aldrich, ~60 mesh, 99%), and Mn<sub>3</sub>O<sub>4</sub> (Aldrich, 325 mesh, 99%) were used as purchased without any purification. Analyses of transmission electron microscopy (TEM) were conducted with JEOL JEM-2010. Scanning electron microscopy (SEM) was carried out with LEO SUPRA 55 (Carl Zeiss, Germany). X-Ray diffraction patterns were obtained by using X-Ray Diffractometer (18 kW) (Mac Science, Japan). Magnetic properties of nanoparticles were measured using superconducting quantum interference (SQUID) magnetometer (Quantum Design, MPMS5XL), which is equipped with a 5 T superconducting magnet. The nitrogen adsorption and desorption isotherms were measured at 77 K using a Micromeritics ASAP 2020 gas adsorption analyzer after the pretreatment at room temperature *in vacuo*. UV absorptions were observed by using V670 UV-Visible-NIR spectrophotometer (JASCO). <sup>1</sup>H NMR spectra were recorded with Jeol 300 MHz spectrometer and referenced to CDCl<sub>3</sub>.

**Synthesis of HMONS.** MnO nanoparticles were prepared by the method described previously with some modifications.<sup>13</sup> In

a typical procedure, 12.4 g of the manganese-oleate complex (2 mmol), prepared by the reaction of MnCl<sub>2</sub>·4H<sub>2</sub>O and sodium oleate in a mixture of ethanol, water and *n*-hexane, were dissolved in 100 g of 1-octadecene. The mixture solution was degassed at 70 °C for 1 h under a vacuum and then heated to 300 °C with vigorous stirring for 1 h. After cooling to room temperature, 20 mL of hexane were added to improve the dispersibility of the nanoparticles, followed by adding 80 mL of acetone to precipitate the nanoparticles. The waxy precipitate was retrieved by the centrifugation. The above purification procedure was repeated to remove excess surfactant and solvent. The purified MnO nanoparticles were dispersed in chloroform. The as-prepared manganese oxide nanoparticles were then transferred into water by modifying a procedure reported previously.<sup>14</sup> Typically, 10 mg of MnO nanoparticles dispersed in 2 mL CHCl<sub>3</sub> (5 mg mL<sup>-1</sup>) were mixed with 5 mL of CHCl<sub>3</sub> solution containing 40 mg of Pluronic F127 and stirred for 30 minutes. Then the solvent was completely removed in vacuum at 80 °C for 1 h. The addition of 5 mL water resulted in a clear and dark-brown aqueous dispersion. Excess Pluronic F127 was removed by ultracentrifugation. The purified nanoparticles were re-dispersed in distilled water and stored for several days, providing the **CSNPs**. In order to carve away the core part and produce **HMONs**, 0.5 mg mL<sup>-1</sup> of **CSNPs** was dispersed in 2.5 M hydroxylamine solution and stirred for 24 h for dissolving away the MnO core. Resulting **HMONs** were retrieved by centrifugation and purified by the repetition of dispersion in distilled water and centrifugation for several times.

**Control experiment with Mn<sub>3</sub>O<sub>4</sub> nanoparticles.** Mn<sub>3</sub>O<sub>4</sub> nanoparticles were synthesized from a previously reported method.<sup>15</sup> In a typical synthesis, a mixture of 0.5 g Mn(acac)<sub>2</sub> and 10 mL oleylamine was placed in a three-necked flask and heated up to 210 °C in open air with continuous stirring for 5 h. After cooling to room temperature, ethanol was added to the reaction dispersion, precipitating the solids of resulting nanoparticles. The precipitated Mn<sub>3</sub>O<sub>4</sub> nanoparticles were retrieved by centrifugation. The Mn<sub>3</sub>O<sub>4</sub> nanoparticles were purified by repeating the re-dispersion in hexane and centrifugation for several times. The Mn<sub>3</sub>O<sub>4</sub> nanoparticles were transferred into the aqueous phase by using same procedure applied for preparing **CSNPs**. The treatment of Mn<sub>3</sub>O<sub>4</sub> nanoparticles in an aqueous hydroxylamine was carried out under the same condition applied for the synthesis of **HMONs**.

**Synthesis of **HMON@*h*-SiO<sub>2</sub>**.** Manganese oxide nanoparticles having a 20 nm of size were prepared through the previously reported procedure in ref. 1. The silica coated manganese oxide nanoparticles (**Mn@SiO<sub>2</sub>**) were made by modification of previously reported reverse microemulsion technique.<sup>16</sup> Polyoxyethylene(5)nonylphenyl ether (0.77 g, 1.74 mmol, Igepal CO-520, containing 50 mol% hydrophilic group) was dispersed in a round bottom flask containing cyclohexane solvent (17 mL). Next, a cyclohexane dispersion (6 mL) of MnO nanoparticles (6 mg) and an ammonium hydroxide solution (30%, 0.13 mL) were successively added with the vigorous stirring to form a translucent dispersion. Lastly, a tetraethyl orthosilicate (TEOS, 0.15 mL) was added and stirred for 12 h. The resulting **Mn@SiO<sub>2</sub>** was precipitated from the reaction dispersion by the addition of

methanol (1 mL) and retrieved by the centrifugation. The crude  $\text{Mn@SiO}_2$ s were purified by repeating the re-dispersion in ethanol and the centrifugation for several times. The purified  $\text{Mn@SiO}_2$ s were re-dispersed in deionized water and stored for further use. For the synthesis of  $\text{HMON@h-SiO}_2$ , 1 mg mL<sup>-1</sup> of  $\text{Mn@SiO}_2$  nanoparticles was treated with 0.5 M  $\text{NH}_2\text{OH}$  solutions at room temperature for 16 h. The resulting  $\text{HMON@h-SiO}_2$  nanoparticles were isolated from the reaction dispersion by the centrifugation and purified by repeating the re-dispersion in water and the centrifugation. The  $\text{Mn}_3\text{O}_4@p\text{-SiO}_2$  used for the control catalytic reaction was prepared by using the  $\text{Mn}_3\text{O}_4$  nanoparticle instead of  $\text{MnO}$  nanoparticle through the same procedure with that applied for the  $\text{HMON@h-SiO}_2$ .

**Determination of solubility of bulk MnO and  $\text{Mn}_3\text{O}_4$ .** 2 mg of bulk  $\text{MnO}$  (Aldrich, ~60 mesh, 99%) and  $\text{Mn}_3\text{O}_4$  (Aldrich, 325 mesh, 99%) powders were individually immersed in 2.5 M  $\text{NH}_2\text{OH}$  solutions and stirred at room temperature. After stirring for 24 h, remaining solids were removed by the centrifugation. And the contents of manganese ions were determined by using ICP.

**Surface modification of  $\text{HMON@h-SiO}_2$ .** The surface modification of  $\text{HMON@h-SiO}_2$  was carried out with several silane surfactants by modifying the previously reported method.<sup>17</sup> For this, four different silane reagents, including (3-aminopropyl)trimethoxysilane, *n*-propyltrimethoxysilane, (2-phenylethyl)trimethoxysilane, and *n*-octadecyltrimethoxysilane, were used. In a typical modification experiment, an ammonium hydroxide solution (30%, 0.45 mL) and a silane reagent (2 mL) were successively added to an ethanol dispersion (30 mL) of  $\text{HMON@h-SiO}_2$ s (100 mg). TEM analyses did not show any significant change in the size and shape of the initial  $\text{HMON@h-SiO}_2$  after the silane modification. While the 3-aminopropyl-, *n*-propyl-, and 2-phenylethyl-modified particles are well dispersible in ethanol or ethanol/water mixture solvent, *n*-octadecyl-modified particles show much better dispersibility in chloroform compared with ethanol or ethanol/water mixture.

### 3.2 Evaluation of catalytic activities of $\text{HMON@h-SiO}_2$ in cyanosilylation reactions

**General procedure for cyanosilylation reactions.**  $\text{HMON@h-SiO}_2$  (**1**) or modified  $\text{HMON@h-SiO}_2$  catalysts (**2a-d**) (0.025 mmol) dispersed in distilled  $\text{CH}_2\text{Cl}_2$  (2 mL) were treated with aromatic aldehyde (0.5 mmol) and cyanotrimethylsilane (0.13 mL, 1.0 mmol) at room temperature under  $\text{N}_2$  atmosphere. After stirring for 12 h, the reaction mixture was filtered through a plunge of Celite and the filtrate was concentrated under reduced pressure to afford the product sample for <sup>1</sup>H NMR analysis. The conversion yields of the reactions were determined by <sup>1</sup>H NMR spectroscopy, and were calculated based on the following representative peaks of aldehyde (ArCHO) and cyanohydrins trimethylsilyl ether (ArCHCN(OTMS)). <sup>1</sup>H NMR (300 MHz,  $\text{CDCl}_3$ ) ppm: 10.02 (**3a**) and 5.50 (**4a**), 10.08 (**3b**) and 5.57 (**4b**), 10.42 (**3c**) and 6.06 (**4c**), 10.81 (**3d**) and 6.35 (**4d**), 11.55 (**3e**) and 6.93 (**4e**), 9.89 (**3f**) and 5.39 (**4f**).

**Competitive cyanosilylation reaction.** *n*-Octadecyl-modified  $\text{HMON@h-SiO}_2$  catalyst (**2d**) (0.02 mmol) dispersed in distilled

$\text{CH}_2\text{Cl}_2$  (2 mL) was treated with benzaldehyde (0.4 mmol), 3,5-bis(benzyloxy)benzaldehyde (0.4 mmol) and cyanotrimethylsilane (3 equiv., 1.2 mmol) at room temperature under  $\text{N}_2$  atmosphere. The NMR spectrum collected at regular intervals to determine the conversion yields.

## 4 Conclusions

In conclusion, a novel selective nanoscale etching process that generated a well defined hollow nanostructure provides a novel method for fabricating a nanoreactor framework consisting of a hollow and porous silica shell and a functionalized interior surface with a catalytically active manganese oxide layer. Furthermore, the nanoreactor fabricated by the newly developed method catalyzes the cyanosilylation reactions with size and shape selectivity, and the size-selectivity effect can be enhanced significantly by engineering the surface of the silica shell.

## Acknowledgements

This research was supported by Basic Science Research Program through the National Research Foundation of Korea funded by the Ministry of Education, Science and Technology (2010-0003950) (ISL) and (2009-0069496) (EJK).

## Notes and references

- 1 For recent reviews on hollow nanoparticles, see: X. W. Lou, L. A. Archer and Z. Yang, *Adv. Mater.*, 2008, **20**, 3987.
- 2 (a) J. Shin, R. M. Anisur, M. K. Ko, G. H. Im, J. H. Lee and I. S. Lee, *Angew. Chem., Int. Ed.*, 2009, **48**, 321; (b) K. Cheng, S. Peng, C. Xu and S. Sun, *J. Am. Chem. Soc.*, 2009, **131**, 10637; (c) X. W. Lou and L. A. Archer, *Adv. Mater.*, 2008, **20**, 1853; (d) J. Gao, G. Liang, B. Zhang, Y. Kuang, X. Zhang and B. Xu, *J. Am. Chem. Soc.*, 2007, **129**, 1428; (e) P. M. Arnal, M. Comotti and F. Schüth, *Angew. Chem., Int. Ed.*, 2006, **45**, 8224.
- 3 For synthesis using sacrificial template, see: X. Huang, H. Zhang, C. Guo, Z. Zhou and N. Zheng, *Angew. Chem., Int. Ed.*, 2009, **48**, 4808; C.-J. Jia, L.-D. Sun, F. Luo, X.-D. Han, L. J. Heyderman, Z.-G. Yan, C.-H. Yan, K. Zheng, Z. Zhang, M. Takano, N. Hayashi, M. Eltschka, M. Kälui, U. Rüdiger, T. Kasama, L. Cervera-Gontard, R. E. Dunin-Borkowski, G. Tzvetkov and J. Raabe, *J. Am. Chem. Soc.*, 2008, **130**, 16968; K. An, S. G. Kwon, M. Park, H. B. Na, S.-I. Baik, J. H. Yu, D. Kim, J. S. Son, Y. W. Kim, I. C. Song, W. K. Moon, H. M. Park and T. Hyeon, *Nano Lett.*, 2008, **12**, 4252; X. Lu, H.-Y. Tuan, J. Chen, Z.-Y. Li, B. A. Korgel and Y. Xia, *J. Am. Chem. Soc.*, 2007, **129**, 1733; D. K. Yi, S. S. Lee, G. C. Papaefthymiou and J. Y. Ying, *Chem. Mater.*, 2006, **18**, 614; Y. Yin, C. Erdonmez, S. Aloni and A. P. Alivisatos, *J. Am. Chem. Soc.*, 2006, **128**, 12671.
- 4 For template-free synthesis, see: (a) X. Liang, X. Wang, Y. Zhuang, B. Xu, S. Kuang and Y. Li, *J. Am. Chem. Soc.*, 2008, **130**, 2736; (b) S. Peng and S. Sun, *Angew. Chem., Int. Ed.*, 2007, **46**, 4155; (c) A. E. Henkes, Y. Vasquez and R. E. Schaak, *J. Am. Chem. Soc.*, 2007, **129**, 1896; (d) J. Gao, B. Zhang, X. Zhang and B. Xu, *Angew. Chem., Int. Ed.*, 2006, **45**, 1220; (e) Y. Yin, R. M. Rioux, C. K. Erdonmez, S. Hughes, G. A. Somorjai and A. P. Alivisatos, *Science*, 2004, **304**, 711.
- 5 S. H. Joo, J. Y. Park, C.-K. Tsung, Y. Yamada, P. Yang and G. A. Somorjai, *Nat. Mater.*, 2009, **8**, 126; J. Lee, J. C. Park and H. Song, *Adv. Mater.*, 2008, **20**, 1523; S. Ikeda, S. Ishino, T. Harada, N. Okamoto, T. Sakata, H. Mori, S. Kuwabata, T. Torimoto and M. Matsumura, *Angew. Chem., Int. Ed.*, 2006, **45**, 7063; J. Li and H. C. Zeng, *Angew. Chem., Int. Ed.*, 2005, **44**, 4342.
- 6 For recent review on engineering of hollow interior space, see: Y. Zhao and L. Jiang, *Adv. Mater.*, 2009, **21**, 3621; U. Jeong, Y. Wang, M. Ibasate and Y. Xia, *Adv. Funct. Mater.*, 2005, **15**, 1907.

- 7 H. Xu and W. Wang, *Angew. Chem., Int. Ed.*, 2007, **46**, 1489; M. Yang, J. Ma, C. Zhang, Z. Yang and Y. Lu, *Angew. Chem., Int. Ed.*, 2005, **44**, 6727; U. Jeong, T. Herricks, E. Shahar and Y. Xia, *J. Am. Chem. Soc.*, 2005, **127**, 1098.
- 8 A. E. Berkowitz, G. F. Rodriguez, J. I. Hong, K. An, T. Hyeon, N. Agarwal, D. J. Smith and E. E. Fullerton, *Phys. Rev. B: Condens. Matter Mater. Phys.*, 2008, **77**, 024403; G. Salazar-Alvarez, J. Sort, S. Suriñach, M. D. Baró and J. Nogués, *J. Am. Chem. Soc.*, 2007, **129**, 9102.
- 9 A. Neaman, B. Waller, F. Mouélé, F. Trolard and G. Bourrié, *Eur. J. Soil Sci.*, 2004, **55**, 47; Y. Thomassen, D. G. Ellingsen, S. Hetland and G. Sand, *J. Environ. Monit.*, 2001, **3**, 555.
- 10 T. Zhang, J. Ge, Y. Hu, Q. Zhang, S. Aloni and Y. Yin, *Angew. Chem., Int. Ed.*, 2008, **47**, 5806; S.-J. Park, Y.-J. Kim and S.-J. Park, *Langmuir*, 2008, **24**, 12134.
- 11 For cyanosilylation reactions with porous metal-organic framework, see: S. Horike, M. Dinca, K. Tamaki and J. R. Long, *J. Am. Chem. Soc.*, 2008, **130**, 5854; O. R. Evans, H. L. Ngo and W. Lin, *J. Am. Chem. Soc.*, 2001, **123**, 10395.
- 12 J. Lee, J. C. Park, J. U. Bang and H. Song, *Chem. Mater.*, 2008, **20**, 5839; S. Ikeda, Y. Ikoma, H. Kobayashi, T. Harada, T. Torimoto, B. Ohtani and M. Matsumura, *Chem. Commun.*, 2007, 3753.
- 13 H. B. Na, J. H. Lee, K. An, Y. I. Park, I. S. Lee, D.-H. Nam, S. T. Kim, S.-H. Kim, S.-W. Kim, K.-H. Lim, K.-S. Kim, S.-O. Kim and T. Hyeon, *Angew. Chem., Int. Ed.*, 2007, **46**, 5397.
- 14 M. Gonzales and K. M. Krishnan, *J. Magn. Magn. Mater.*, 2007, **311**, 59; T. K. Jain, M. A. Morales, S. K. Sahoo, D. L. Leslie-Pelecky and V. Labhasetwar, *Mol. Pharmaceutics*, 2005, **2**, 194.
- 15 D. C. Lee, V. F. Mikulec, J. M. Pelaez, B. Koo and B. A. Korgel, *J. Phys. Chem. B*, 2006, **110**, 11160; D. K. Yi, S. T. Selvan, S. S. Lee, G. C. Papaefthymiou, D. Kundaliya and J. Y. Ying, *J. Am. Chem. Soc.*, 2005, **127**, 4990.
- 16 F. Jiao, A. Harrison and P. G. Bruce, *Angew. Chem., Int. Ed.*, 2007, **119**, 4020.
- 17 Y. Piao, J. Kim, H. B. Na, D. Kim, J. S. Baek, M. K. Ko, J. H. Lee, M. Shokouhimeher and T. Hyeon, *Nat. Mater.*, 2008, **7**, 242.